Astron. Astrophys. 274, 627–641 (1993)

ASTRONOMY AND ASTROPHYSICS

A survey of the dynamics of main-belt asteroids. I

R. Dvorak[1], **P. Müller**[2], **and J. Kallrath**[3,4]

[1] Institute of Astronomy, University of Vienna, Türkenschanzstrasse 17, A-1180 Vienna, Austria
[2] Max-Planck-Institut für Radioastronomie, Auf dem Hügel 69, W-5300 Bonn 1, Germany
[3] Astronomische Institute der Universität Bonn, Auf dem Hügel 71, W-5300 Bonn 1, Germany
[4] BASF-AG Abt. ZXT/C, Kaiser-Wilhelm-Str. 52, W-6700 Ludwigshafen, Germany

Received May 18, 1992; accepted March 1, 1993

Abstract. We present a survey of the dynamical structure of the main asteroid belt between Mars und Jupiter. The results are displayed as 3-dimensional plots showing the dynamical evolution of fictitious asteroids with initial semimajor axes ranging from 0.3 to 0.8 (in units of the semimajor axis of Jupiter's orbit) which includes all the existing main belt asteroids. The initial eccentricity of these bodies was fixed between 0.0 and 0.25 which is in the most interesting range. We chose a mesh with a grid width in initial semimajor axis $\Delta a = 0.002$ and $\Delta e = 0.025$ in initial eccentricity. The orbits of about 3500 fictitious asteroids (2750 are shown in the graphs) were integrated numerically over 10^4 Jupiter periods corresponding to approximately 10^5 years. We take the standard deviations σ of the semimajor axis a, eccentricity e and inclination i, as parameters characterizing the orbital perturbations due to Jupiter. These $\sigma(a), \sigma(e), \sigma(i)$ are plotted as functions of the initial conditions a and e. All the main perturbations associated with the mean motion resonance are well reproduced. These results are compared to existing numerical ones and also to recently derived analytical developments. Furthermore, our results do not only reproduce the actual distribution of the main belt asteroids with respect to the semimajor axis, but also reveal some "new" resonances which are manifested through larger deviations of the three elements mentioned.

Key words: main belt asteroids – kirkwood gaps – Hildas – elliptic restricted problem

1. Introduction

The explanation of the dynamical structure of the main belt of asteroids between Mars and Jupiter has been a challenging problem since the discovery of the Kirkwood gaps. Although it was possible to identify the location of the gaps in the real asteroid distribution (=RAD, Fig. 1) with the mean motion resonances of the asteroids with Jupiter, the scenario of the depletion remained a puzzle for more than 100 years and it is still being discussed. Different hypotheses have been developed: e.g., the statistical approach, a pure gravitational theory, the collisional hypothesis, the cosmogonic hypothesis and the primeval sweeping (Scholl 1979, 1985; Ferraz-Mello 1987, 1990). No clear answer has yet emerged although more and more pieces of the puzzle have been correctly assembled.

In our paper we briefly discuss existing numerical and analytical results of the problem. We then explain our computational method and the choice of the initial conditions. The presentation of the results is in form of three - dimensional plots showing the perturbations of Jupiter on the orbital elements of the fictitious asteroids as functions of the initial values of the semimajor axis and the eccentricity. Every resonance (which may or may not be identified with a gap in the real distribution of asteroids) is discussed separately after the presentation of the global results. Questions, still open, are enumerated and future projects are presented briefly.

It is definitely not our purpose to explain all details of the dynamical structure of the gaps; we plan this in another publication where Saturn's gravitational force will be examined in detail. The main task is rather to display the numerical results in the framework of the three - dimensional elliptic restricted problem for reference purposes which may be interesting for other investigators in the area.

2. The present status

A big step toward the understanding of the Kirkwood gaps was achieved when the orbits of asteroids in the gaps were integrated numerically. This approach produced interesting results only after computers became fast enough to cover the lifetime of such bodies. (e.g., Froeschlé & Scholl 1981, 1982). The most important contribution to the understanding of the origin of the gaps was the discovery of chaotic motions in the 3:1 resonance with Jupiter in the main belt of asteroids by Wisdom (1982, 1983), who derived his results using a mapping method within the framework of the averaged elliptic restricted problem. This

Send offprint requests to: R. Dvorak

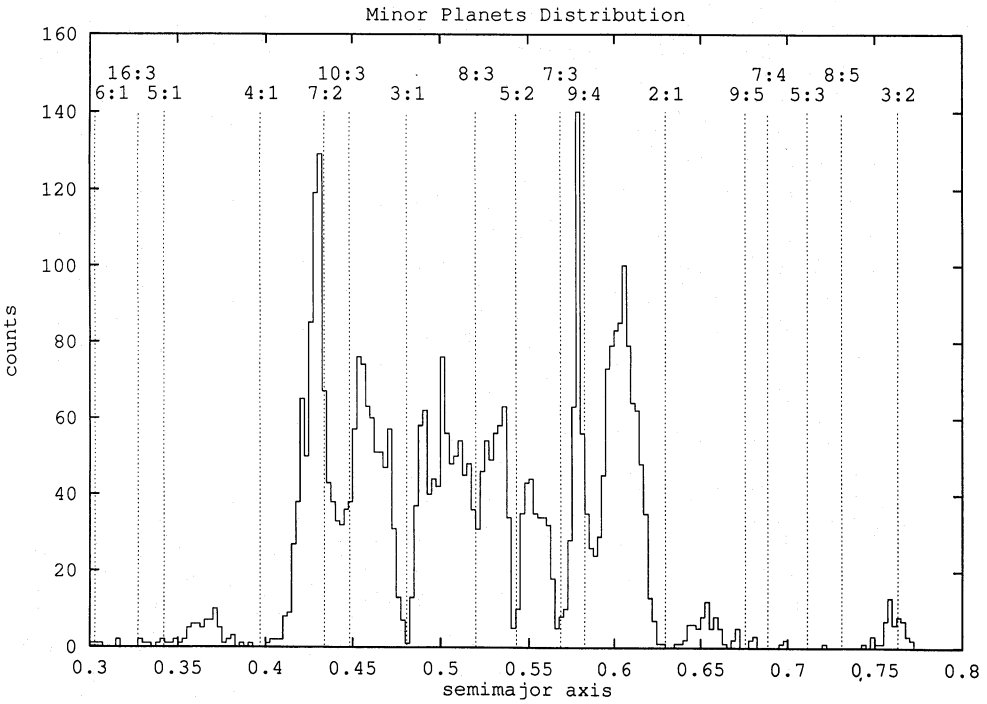

Fig. 1. The real distribution of 4207 members of the main belt asteroids = RAD. The resonances are indicated with dashed lines

technique is much faster than any classical numerical integration and can cover time periods up to millions of years in relatively short computing time. After a long time period of moderate changes in the eccentricity ($0 \leq e \leq 0.1$), a sudden increase up to $e = 0.4$ of two orbits was discovered. The asteroid thus became a possible Mars crosser, consequently – after a close approach to Mars – it may escape sooner or later from the resonance. This phenomenon – sudden quantitative changes – is commonly observed in nonlinear dynamics and in recent years has been a major research topic in theoretical mechanics. Considerable progress has been achieved ever since appearances of chaos in planetary dynamics were first noticed: e.g., by Laskar (1987) for the planetary motions and by Chirikov & Vecheslavov (1986), Petrosky & Broucke (1988), Froeschlé & Gonczi (1988) and Dvorak & Kribbel (1990) for comets.

Various investigators have succeeded in modeling specific gaps through analytical perturbation theory: developments of the perturbation function up to a certain order, canonical transformations and averaging techniques were used to reduce the problem to a system two degrees of freedom.

Some specific gaps (11:3, 7:2, 3:1, 2:1, 5:3, and 3:2) were studied in the framework of the circular restricted three-body problem using Peridic Orbits and the method of surface of section by Hadjidemetriou & Ichtiaroglou (1984). They found that there are gaps at the 3:1 and 5:3 resonances and families at the 2:1 and 3:2 resonances, but very close to the 1^{st} order resonances there are gaps.

Giffen (1973) used Schubart's averaging (Schubart 1968) in the elliptic restricted problem for the 2:1 resonance and found a small zone of "very complex motion" which "might be related to the formation of gaps". Ferraz-Mello (1988) studied highly eccentric librators in the Hilda case and found that they cross the 2:1 gap. Recently, Lemaitre & Henrard (1990) developed a semianalytical method for the 2:1 resonance and concluded that their results do "not support the theory of formation of the 2:1 Kirkwood gap by removal of the asteroids through close encounters with Mars". A new analytical treatment by Morbidelli & Giorgilli (1990) could find "no mechanical explanation in the framework of the complete restricted problem of three bodies" for the 2:1 Kirkwood gap.

There exists a complete study using Wisdom's mapping method by Murray & Fox (1984) for the 3:1 resonance, in which the structure of the gap was determined by examining the orbit's chaoticity with the Lyapunov exponents. The separation of the chaotic domain, which exists for e_{ini}=0, into two for higher values of $e = 0.4$ is mainly a consequence of the secondary resonances (Henrard & Caranicolas 1990). Yoshikawa (1990) also found the structure of the gap in his analytical and numerical approach. The highly eccentric motions in this gap were also studied by Ferraz-Mello & Klafke (1991) and for other resonances by Klafke et al. (1992). In the present study we concentrate on orbits of initially low eccentricity (up to $e = 0.25$)

The practical use of mapping methods for motions near resonances was shown by Hadjidemetriou (1986, 1988, 1991), where especially the 3:1 resonance was examined in detail; here chaotic motion of an asteroid with the characteristic of sudden jumps of the eccentricity up to high values was also found.

Very recently Dvorak (1992a) published results showing the dynamical structure of the 3:1 and 2:1 resonances, which are in good agreement with the existing knowledge. One new result was the discovery of very strong perturbations on one edge of the 2:1 resonance (close to Jupiter) where large eccentricity fluctuations occur even for orbits of the fictitious asteroids with small initial eccentricities.

For the important 2:1, 3:1, 5:2 and the 7:3 resonances (which are quite well visible in the real asteroid belt as gaps, and are almost completely depleted, Fig. 1) , there also exists important numerical and semi-numerical work by Yokishawa (1989, 1990, 1991). His results explain the origin of the Kirkwood gaps at the 3:1 and 5:2 resonances by an increase in the asteroid's eccentricity of the asteroid (then a close approach with one of the planets can kick the asteroid out of the resonance). This may not be the cause for the lack of asteroids in the 2:1 and 7:3 resonances, which show relative broad zones of small perturbations in the middle of the resonance (relatively confirmed in our study). Detailed results for individual orbits are shown for other resonances and discussed in connection with libration and circulation of the critical argument and also the maximum eccentricity variations for each resonance (again only for individual orbits) are given.

Quite an interesting study was recently presented by Šidlichovský (1992a,b) in which he investigated the chaotic behavior of the asteroids' motion in higher resonances with the aid of a mapping method and surfaces of section. The results were very useful for understanding the existence of the nonzero minimum value for the eccentricity (see Sect. 4).

New results by Gladman & Duncan (1990) and by Lecar et al. (1992) for the outer main belt asteroids will be discussed in Sect. 8.

3. The method

The framework of our computations is defined by

- the dynamical model
- the method for the numerical integrations
- the time scale of the integration
- the initial conditions
- the grid size in the initial semimajor axis and the initial eccentricity

At first we had to decide which dynamical model to use. It is evident that the principal cause of the distribution of the known asteroids in the belt, e.g., the gaps and the families, is due to Jupiter perturbing the orbits. Moreover, it has been known since Wisdom's work (1983) that without the eccentricity of Jupiter's orbit, asteroid orbits cannot escape from a resonance. This was again tested recently by Dvorak (1992a) in the 3:1 mean motion resonance using numerical integrations where two models were compared: assuming the circular restricted three-body problem as dynamical model, the eccentricity of the fictitious asteroid ranged within $0.1 \leq e \leq 0.25$; but when the elliptic problem was used as model the asteroid's eccentricity reached maximum values up to 0.4 for the "same" initial conditions. These may be explained as follows: when the eccentricity of Jupiter's orbit is ignored, the zero velocity curves, defined by means of the Jacobian Integral, prevents an increase in eccentricity.

We therefore decided to base our calculations on a dynamical model known as the elliptic restricted problem in three dimensions (Szebehely 1970), with Jupiter in an unperturbed eccentric orbit (e=0.048) around the sun ($m_{jupiter}/m_{sun}$ = 1./1047.355)

Concerning the numerical integration method, we tested various integrators and concentrated on the Lie-integration method and the Schubart-Stumpff (Schubart & Stumpff 1966) extrapolation with variable step size. Other algorithms such as the one by Bulirsch & Stoer (1966) and the classical Runge Kutta had been compared to the Lie-integrator by Dvorak & Kribbel (1990). The Lie-integration program was already been used for many calculations in Planetary System dynamics (e.g. Dvorak & Lohinger 1991) and discussed in great detail by Hanslmeier & Dvorak (1984). It has variable step size and the precision was kept at 10^{-12} for the Lie-Terms (12^{th} order), corresponding to a precision of 14 digits from one step to the next . The customary tests (different step sizes, integration into the future and back to the initial time) produced very satisfactory results.

Considering both precision and computational speed, we found the Lie-integration method the most suitable and therefore used it for this survey.

The time scale had to be chosen such that the results derived for the $\sigma(a)$,$\sigma(e)$ and $\sigma(i)$ did not depend on the integration time in the sense that a change in the duration of integration will not change exceedingly the outcome. We selected 10^4 Jupiter periods (corresponding to more than 10^5 years) as an acceptable compromise between a still tolerable computer-time for the integration of 2750 fictitious orbit and the "accuracy" of the results (the standard deviations of the elements). Over this time scale, the phenomenon of sharp peaks in the time evolution of the asteroid's eccentricity is also quite pronounced (Dvorak 1992a, 1992b). Furthermore the time scale chosen is equivalent to Wisdom's integrations (Wisdom 1987) and ensures the inclusions of most longperiodic perturbations. It also reveals the principal features of the dynamical evolution of asteroids in the main belt, except for phenomena that occur only in highly eccentric orbits (Ferraz-Mello & Klafke 1991).

Other parameters to adopt were the initial values of the mean anomalies M (whether to start with the bodies in conjunction or in opposition) and the initial arguments of the perihelia. Ideally we should determine the critical angles $\psi = (p+q).\lambda_1 - p.\lambda$ (where q is the order of the resonance) which are related to the usual canonic resonance variables (e.g. Ferraz-Mello 1988). We checked the results only for different mean anomalies of the fictitious massless asteroid and set all other angles initially to zero. This means that we fixed $\lambda_{Jupiter} = 0$ and only carried out the test calculation for different values of the mean anomaly of the fictitious asteroid. This was done for two different cases: no differences were apparent for the 3:1 resonance, but we found a strong dependence on the initial conditions for the 2:1 resonance. It should be mentioned that the initial conditions adopted in this way (all the angles equal to 0) correspond to a conjunction with the asteroid at the perihelion of its orbit. For the odd order resonances (2:1, 3:2, 4:1, 5:2, etc.), this means that the asteroid is protected from an immediate close approach to Jupiter if the conjunction takes place at the aphelion of its orbit. For the resonances of even order (3:1, 7:3, etc.), however, closer conjunctions can occur shortly after the beginning of the runs. For the present study we nevertheless fixed $\lambda_{Jupiter} = 0$ and also $\lambda_{asteroid} = 0$ for all resonances relying on another study

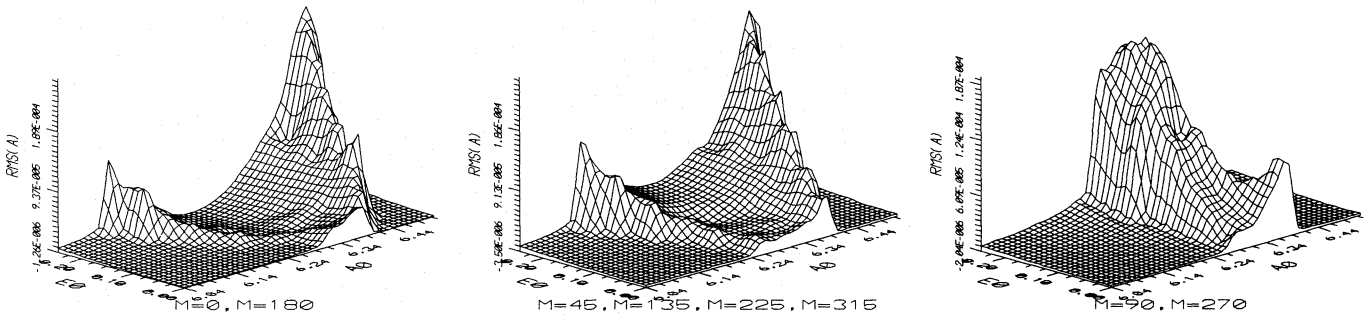

Fig. 2. Structure diagrams for the 2:1 resonance with different mean anomalies. x-axis is the initial semimajor axis in $10 \cdot IU$, y-axis is the initial eccentricity and z-axis is the mean standard deviation for a, $\sigma(a)$. The integration period was always 10^4 Jupiter periods

in progress for checking the details of the differences between the 2:1 and 3:2 resonance.

Another important parameter is the initial inclination between the orbital planes of the bodies. The rôle of the inclinations will here not be discussed in detail, however, because we concentrated on low inclination orbits which show only a very limited sensitivity to the inclinations. But in spite of that, the $\sigma(i)$ is a good indicator of the magnitude of the perturbations acting on the asteroid.

Also important was the grid size for the initial values of the asteroids' orbits. On the one hand we wanted to be sure that the work uncover most of the dynamical structure of the belt (thus requiring a very small grid in semimajor axis and eccentricity). Clearly a denser net of initial conditions would improve the resolution of our results. On the other hand with the fineness of the grid the computer time required increases and we wanted to keep it within reasonable limits. As a compromise we, worked with a grid of $\Delta a = 0.002$ (normalized to Jupiter's fixed semimajor axis, which is the unit chosen for this paper = IU) for values of the semimajor axis between 0.3 and 0.8. This corresponds to a sequence of 250 different values of a_o for the fictitious asteroids.

The grid size in eccentricity was fixed to $\Delta e = 0.025$, so that there are 11 values for each a from e=0.0 to e=0.25 . Consequently, 2750 fictitious asteroids were used in our numerical experiment. The comparison of the results for the 2:1 resonance shown in Fig. 2 with those previously found (cf. Fig. 15 Wisdom 1987, or Fig. 10 of Henrard & Lemaitre 1986) shows that the grid size chosen for our survey is sufficient to reflect the real structure.

Figure 2 in addition shows the comparison for the dynamical structure of the 2:1 resonance for different initial mean anomalies. No bifurcation is seen for $M = 90^o$ and $M = 270^o$.

To summarize the framework for our calculations of the dynamics of the main belt asteroids:

- The dynamical model is the three dimensional elliptic restricted problem.
- The calculations are carried out with the Lie-integrator.
- The duration of integration is 10^4 Jupiter periods $\sim 1.2 \cdot 10^5$ years.
- The initial mean anomaly of Jupiter $M_J = 0$.
- The initial mean anomaly of the asteroid $M = 0^o$.
- The longitude of the perihelion $\omega_o = 0^o$.
- The initial inclination of the asteroid $i_0 = 15^o$.
- The grid in eccentricity is $\Delta e = 0.025$.
- The grid in semimajor axis is $\Delta a = 0.002\ IU$.

Another question must be discussed before we interpret the results: should the bodies be withdrawn from the survey when there is a possibility of crossing Mars' orbit? We decided to retain them in the statistics because removing them would be an artificial intervention of the elliptic restricted problem which was chosen as a model. Nevertheless, when one seeks to understand the depletion in the gaps and to explain the "real" distribution function (like the RAD), the escaped asteroids must in fact, be removed.

Another point must be clarified: when a special resonance is inspected, it is useful to follow single orbits and to look at the critical angles involved. This was undertaken in the above quoted paper by one of us for the 2:1 and 3:1 resonance (Dvorak 1992a). It will not be done in this survey, which was undertaken to derive global results of the dynamics of main belt asteroids.

4. Survey of the dynamical structure

To determine the dynamical structure of the belt we had to find a method to illustrate the perturbations of Jupiter acting on the asteroids. One way is to plot the highest values of the eccentricity occurring during the integration time (cf. Murray 1986 and Dvorak 1992a, 1992b), another, to plot the standard deviations of the three elements: semimajor axes, eccentricity and inclination, ($\sigma(a)$,$\sigma(e)$ and $\sigma(i)$) versus the grid of initial conditions (a_o and e_o) described in the preceding section. This method shows how the elements develop over the whole integration time; greater values of σ evidently correspond to greater perturbations of Jupiter. Especially important for the dynamical evolution of an asteroid is the eccentricity: a highly eccentric orbit can suffer from close approaches to Jupiter itself or (but such orbits are not taken into account in this study) with other planets. It is well known that the semimajor axis can change drastically after such an event (as do the other elements). This scenario is a possible cause of the depletion of asteroids at special locations (resonances) in the main asteroid belt (e.g., Henrard, Scholl, Froeschlé, Wisdom and others, loc.cit.).

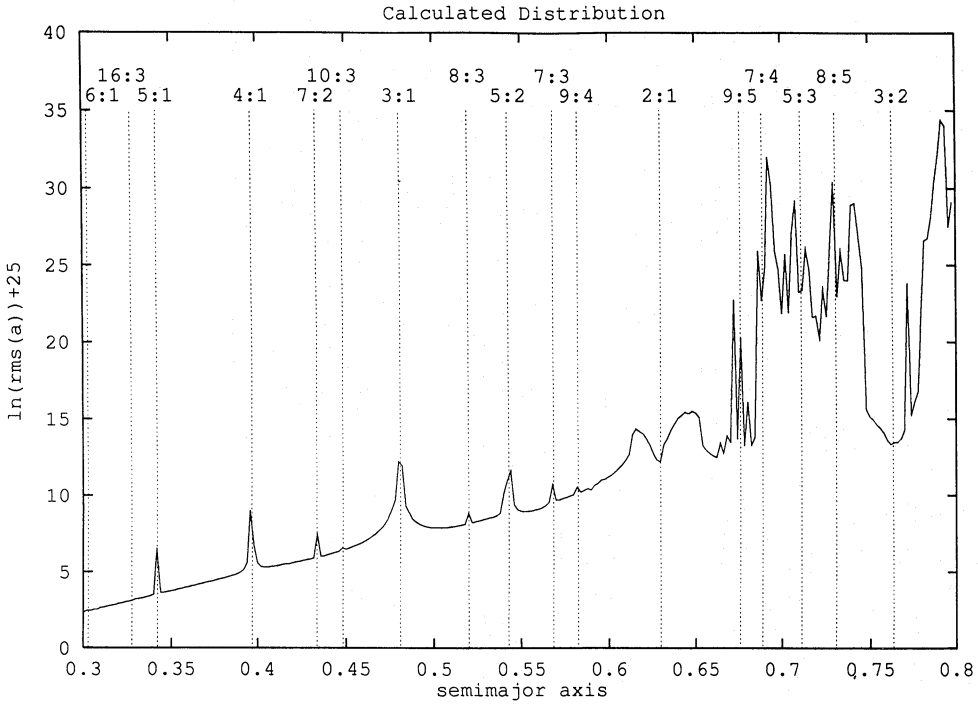

Fig. 3. Spectrum of the dynamical structure of the main belt asteroids in $\sigma(a)$. This spectrum shows the values of $\ln(\sigma(a))$ averaged over all initial eccentricities e. The resonances are indicated with dashed lines. Note the mean linear increase of $\sigma(a)$ in the logarithmic plot

The plots (Figs. 3, 4 and 5) for the $\sigma(a)$,$\sigma(e)$ and $\sigma(i)$ against the initial semimajor axis a_o (without paying attention to the differences in $0 \leq e_o \leq 0.25$) show the features that can be identified with the gaps of the RAD (Fig. 1). We notice that in the inner belt each resonance (5:1, 4:1, 7:2, 3:1, 8:3 5:2, 7:3 and 9:4) manifests itself as a peak in the standard deviation. For the outer belt resonances (2:1, 7:4, 5:3, 8:5 and 3:2) we see a local minimum of σ at the exact location of the resonance, while the edges show large σ values. This behavior is especially pronounced for the 2:1 gap and the 3:2 family; again it is, at this point, not possible to explain the difference between the gaps and the families. A very strong correlation between the perturbations in the three elements a, e and i is also evident, as inferred from the location of similiar structures in the three plots. We nevertheless recognize that the standard deviation of the eccentricity and inclination in the inner belt is large only (a peak in the diagrams 4 and 5) at the 3:1 and 5:2 resonances. The outer belt structure of $\sigma(e)$ and $\sigma(i)$ is similar to that of the $\sigma(a)$: local minima at the exact locations of the resonance.

When looking for more details, we investigate groups according to the value e_o of the initial eccentricity and use a smaller scale (Figs. 6 to 9); there are obviously many interesting differences in the $\sigma(a)$,$\sigma(e)$ and $\sigma(i)$ diagrams. It should be emphasized that the different plots in Figs. 6-9 may be misleading when we compare them to the overall diagrams of Figs. 3-5 in which all eccentricities were lumped together. The z-axis of all the 3 - dimensional plots is always scaled from minimum to maximum value to provide maximum structure resolution. The z-scaling may be quite different from one plot to the next (up to 10^2 in σ).

The $\sigma(e)$ and the $\sigma(i)$ are generally larger for higher initial eccentricities (apparent as an inclined plane toward the value $e_o = 0$). This feature is also present in the $\sigma(a)$-diagram but less evident there (smaller slope of the main plane).

Since the perturbations generally increase from the inner to the outer part of the belt, the structures are more pronounced in the inner belt (up to the 2:1 resonance). Actually, only a few (about 50) asteroids are between the 2:1 resonance and the strongly acting 9:5 resonance as well as the other ones (7:4, 5:3 etc.). Globally, the outer edge of the belt is difficult to classify because of the emergence of ever more high order resonances close to each other. In spite of that, the Hilda valley (with about 50 actual members) is the last region not influenced by large perturbations.

An interesting feature appears in the $\sigma(e)$ diagrams on the finer scale of the inner edge and also on the fine scaled diagram of the Hilda valley: the absolute minimum does not occur at $e_o = 0$ but around $e_o = 0.025$. The reason for this was explained by Šidlichovský (1992a,b) in the above mentioned papers where he found that a stable equilibrium point in the surface of section is located at a value $e \neq 0$ in high order resonances. A finer division in e should be used for a detailed analysis of this minimum. This minimum is also present in main Kirkwood gaps (3:1, 5:2 and from the 2:1 on), but the scale is too large to see it clearly.

Note also the occurence of a phenomenon we call "inversion": Some of the resonances visible in the $\sigma(a)$ as mountains appear as local minima in the $\sigma(e)$. This inversion is especially well developed for 5:1, 8:3; it appears also in the 7:3 and 9:4 resonances. Translated into the language of stability, this means that the eccentricities of the orbits there are less changed by perturbations at the exact resonance than when a_o is only close to the accurate resonance value.

There are two pits in the representation of the inner belt: one in $\sigma(a)$ and the other in $\sigma(i)$. These sets of special initial values

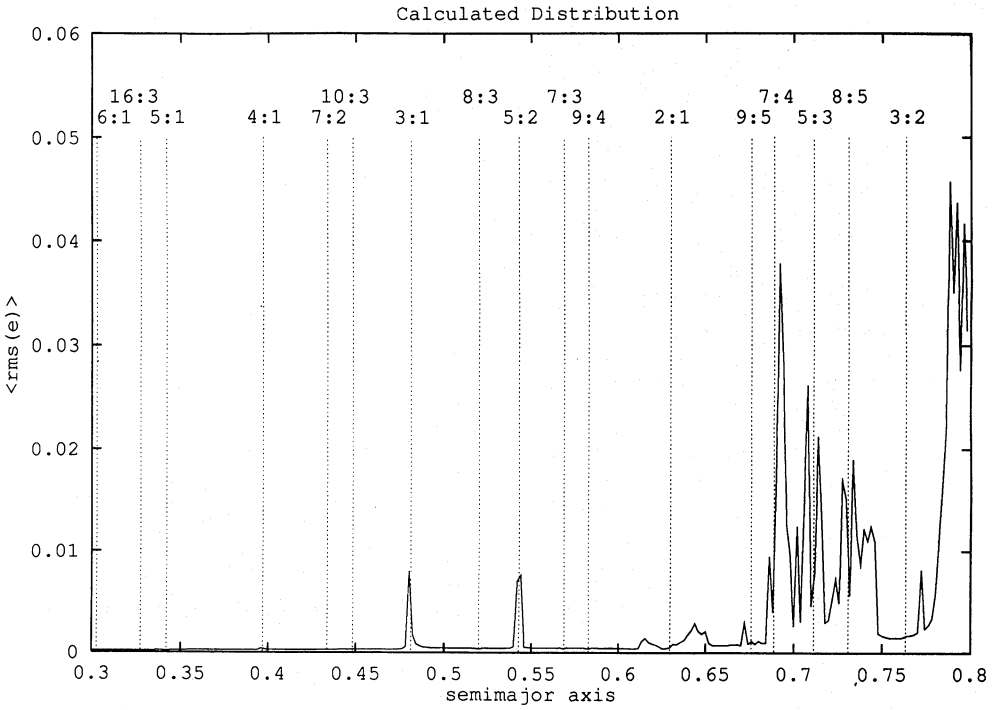

Fig. 4. Spectrum of the dynamical structure of the main belt asteroids in $\sigma(e)$. This spectrum shows the values of $\sigma(e)$ averaged over all initial eccentricities e. The resonances are indicated with dashed lines

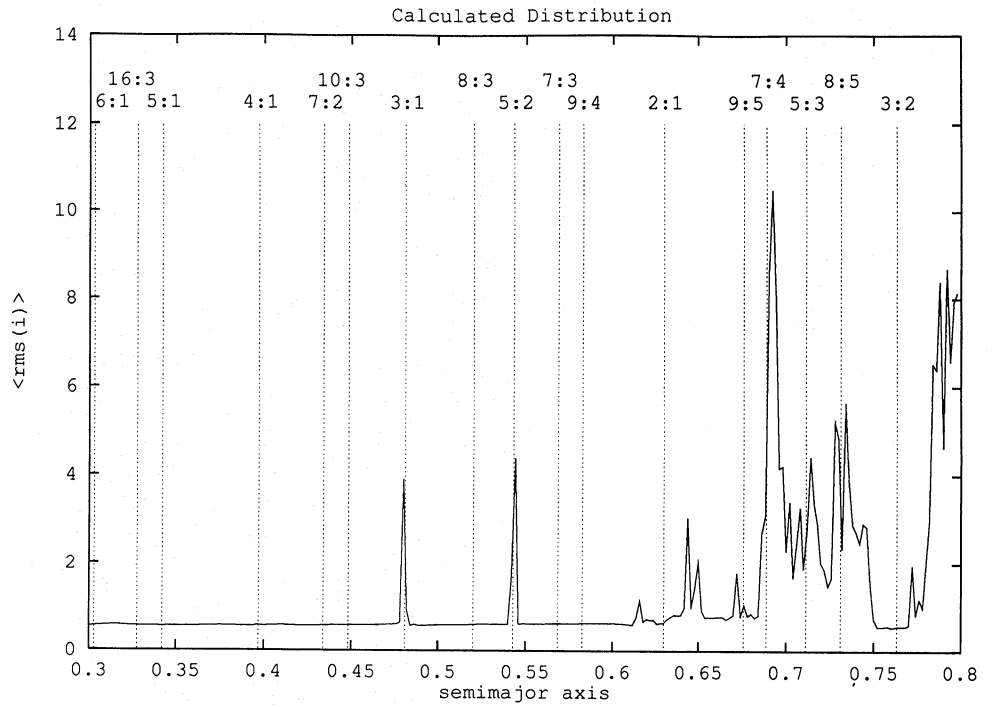

Fig. 5. Spectrum of the dynamical structure of the main belt asteroids in $\sigma(i)$. This spectrum shows the values of $\sigma(i)$ averaged over all initial eccentricities e. The resonances are indicated with dashed lines

lead to an orbit more stable than outside the resonance. We have no dynamical explanation for this seemingly anomalous phenomenon.

Following the increasing semimajor axis in the plots for $\sigma(i)$ (Figs. 6-9), a small amplitude wave (A($\sigma(i)$ = 0.5)) occurs with a decreasing period of $\Delta(a) \geq 0.05\ IU$. It seems that the phase of this wave depends on the eccentricity.

An accurate analytical theory for the motion of the main belt asteroids – regrettably not available at this time – must be capable of explaining all these features. The construction of an analytical theory for every gap and the Hildas (3:2 family) may be possible through parameter fitting to the differential equation driving the resonance (e.g. Bock 1987; Bock et al. 1988; Kallrath 1992).

5. Possible "new" (high-order) resonances

Sometimes the graphs (Figs. 6-9) show small features (small perturbations) in the plane of the main belt (motion "free" of

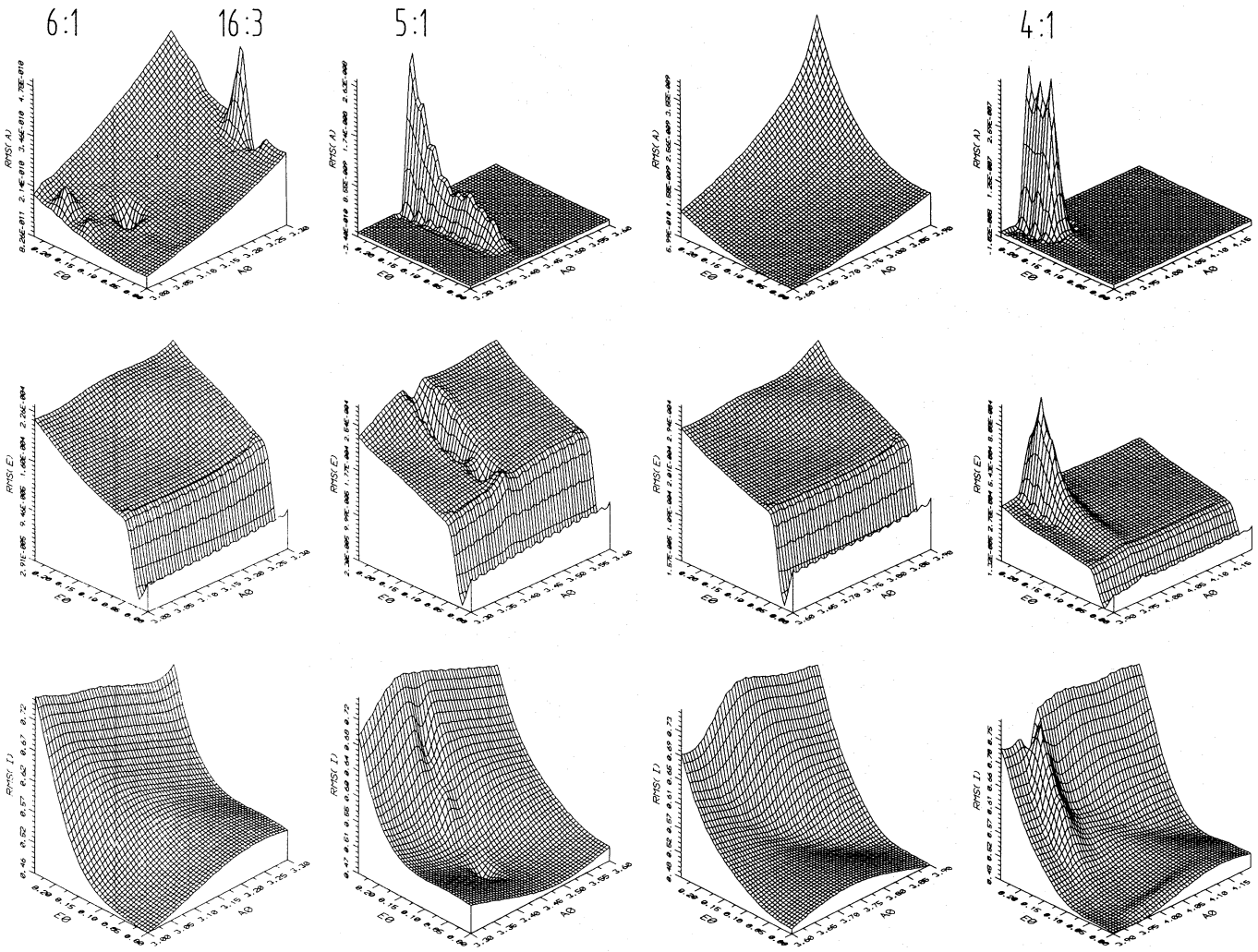

Fig. 6. Detailed picture of the dynamical structure of the main belt asteroids I. The x-axis shows the initial semimajor axis in IU scale by a factor 10. The y-axis shows the initial eccentricity and the z-axis shows the mean standard deviation of the elements a, e, i. Note: The scale of the z-axis differs from plot to plot

resonances) that cannot be explained by the main resonances; these may be due to high-order resonances. They are not always visible in all three diagrams ($\sigma(a) - \sigma(e) - \sigma(i)$) sometimes we find the suggestion for a perturbation acting on only one element. Starting from the inner belt (the figures should be read from left to right) we briefly describe these features visible as "hills", "pits" and "inversions".

- Figure 6a: A small hole in the $\sigma(a)$-diagram is visible close to the 6:1 resonance on the inner edge at a = 0.303 around e = 0.12. Starting with these initial values leads to an orbit with nearly constant semimajor axis. Such a small region of no perturbation is not present in either in the $\sigma(e)$- or the $\sigma(i)$-diagram The location of the pit is very close to the **41:7 resonance**.
- Figure 6a: A higher perturbation peak arises in the $\sigma(a)$-diagram at a = 0.328IU, e = 0.12, but again is not visible in the other two elements. The location of the "hill" is most likely the **16:3 resonance**.
- Figure 7a: We find a small peak for $e_o \geq 0.15$ in $\sigma(a)$ on the outer edge of the 7:2 resonance at a = 0.448. The location is at the **10:3 resonance**.
- Figure 8a: On the outer side of the 9:4 resonance, a small inversion is visible in the $\sigma(a)$- and $\sigma(e)$-diagrams for $e_o \geq$ 0.17 (maybe a "pit" in a). This indicates an orbit more stable with respect to the semimajor axis and the eccentricity, but not the inclination. The location can be identified with the **11:5 resonance** (a = 0.591).

As already mentioned the phenomenon of resonance overlap makes it difficult to distinguish properly small deviations from the 2:1 resonance on. It should be emphasized, that $\sigma(a)$ for most of the listed "new " resonances is, in fact, very small and about two orders of magnitude below the $\sigma(a)$ of the Griqua gap.

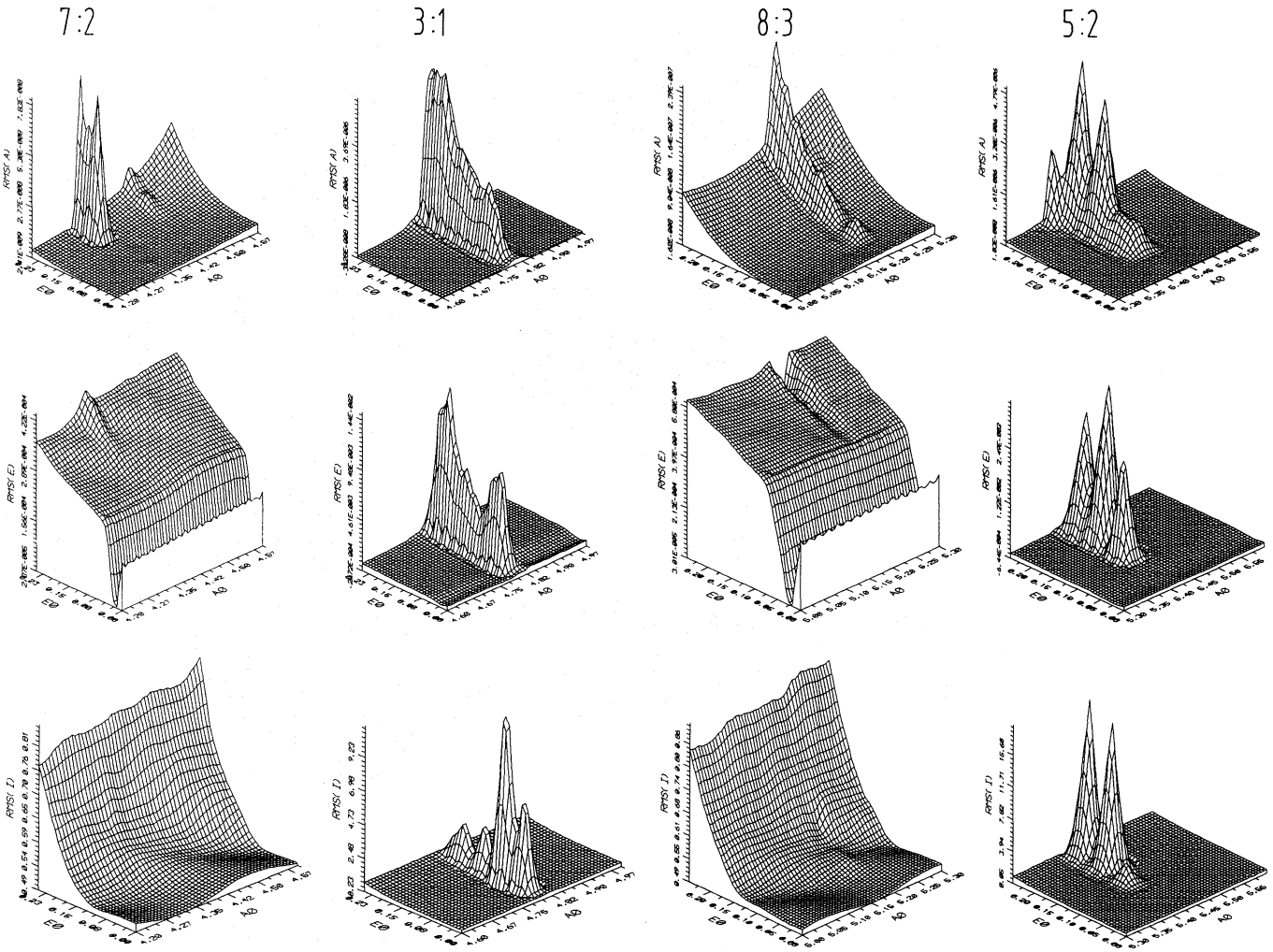

Fig. 7. Detailed picture of the dynamical structure of the main belt asteroids II. The x-axis shows the initial semimajor axis in IU scale by a factor 10. The y-axis shows the initial eccentricity and the z-axis shows the mean standard deviation of the elements a, e, i. Note: The scale of the z-axis differs from plot to plot

6. The main resonances

Starting from the inner main belt, we now describe each main resonance. Some of them have already been studied numerically and/or analytically by other authors as was pointed out in previous sections of this paper.

6.1. The 6:1 resonance (a = 0.303)

(Fig. 6a): This weak resonance is visible only in the $\sigma(a)$-diagram through a very small peak ($\sigma(a)_{max} = 2 \cdot 10^{-10}$) from e=0.10 to e=0.20. Only 2 asteroids are present around this resonance in the RAD.

6.2. The 5:1 resonance (a = 0.342)

(Figure 6b): This resonance is well defined in the $\sigma(a)$-diagram by a steep "mountain" from $e_o \geq 0.05$ ($\sigma(a)_{max} = 3 \cdot 10^{-5}$). One recognizes surprisingly a valley of smaller perturbation at exactly the same location in the $\sigma(e)$-diagram. The inversion is nearly invisible in the $\sigma(i)$-diagram, but may cause a pit for e_o = 0.075. This inversion may be responsible for a stabilization of the motion of the asteroids in this region: some 10 asteroids are in fact found around this resonance in the RAD.

6.3. The 9:2 resonance (a = 0.367)

(Figure 6c): This resonance is not at all detectable in the plots and lies embedded in the big valley between the 5:1 and 4:1 resonances. The valley in the RAD is populated with a family of asteroids as numerous as the Hilda family.

6.4. The 4:1 resonance (a = 0.397)

(Figure 6d): We see the relatively large perturbation mainly in the $\sigma(a)$-diagram ($\sigma(a)_{max} = 4 \cdot 10^{-7}$) for $e_o \geq 0.15$. The perturbation is also visible in the $\sigma(e)$-diagram and $\sigma(i)$-diagram (starting with smaller e-values). In i, it appears as a broad, smooth plane and then as a relatively sharp, but not high, peak

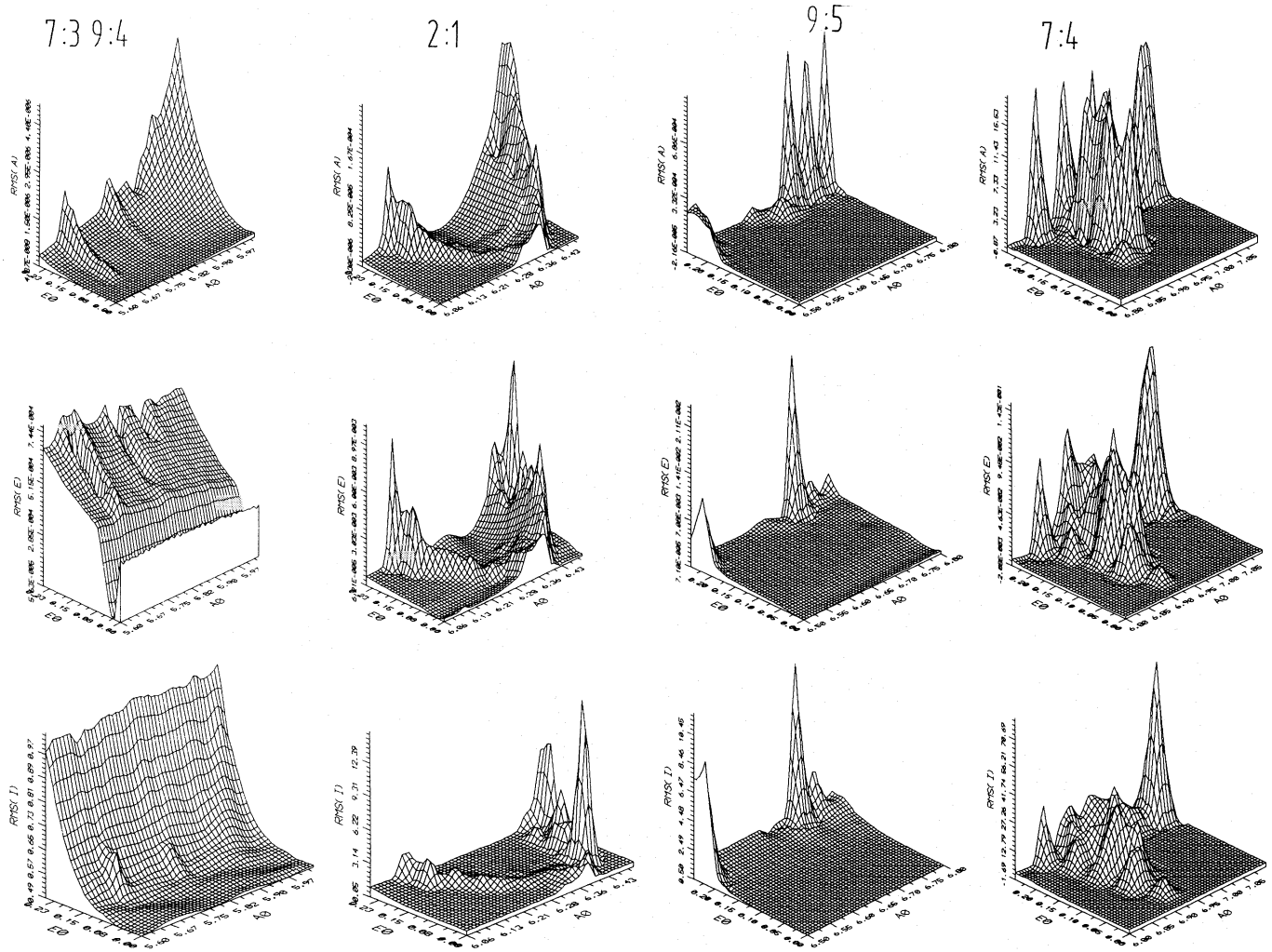

Fig. 8. Detailed picture of the dynamical structure of the main belt asteroids III. The x-axis shows the initial semimajor axis in IU scale by a factor 10. The y-axis shows the initial eccentricity and the z-axis shows the mean standard deviation of the elements a, e, i. $\sigma(a)$ is cut off at 20 IU. Note: The scale of the z-axis differs from plot to plot

up to e = 0.2; at higher e-values we see again an inversion. This resonance is a well-defined gap in the RAD (there are no asteroids close to that resonance).

6.5. The 7:2 resonance (a = 0.434)

(Figure 7a): This resonance is well defined in our diagrams: As a relatively sharp peak ($\sigma_{max} = 7.5 \cdot 10^{-8}$) in the $\sigma(a)$-diagram, as a very small peak only for high e-values in the $\sigma(e)$-diagram and absent in the $\sigma(i)$-diagram. This gap is not well defined in the RAD (some hundred asteroids are close to that resonance), but it is visible as a local minimum in Fig. 1 in between the 7:2 and 10:3 resonance. Our numerical results fail completely to explain this feature.

6.6. The 3:1 resonance (a = 0.481)

(Figure 7b): This major Kirkwood gap has been extensively discussed in the literature and explored with the aid of numerical experiments and analytical models. It is easily visible in all three diagrams and broadens toward higher initial e-values ($\sigma(a)_{max} = 5.5 \cdot 10^{-6}$). The bifurcation predicted by the theory is not apparent. Nevertheless, the principal feature can be discovered as sharp increases of the eccentricities up to e=0.4. As mentioned above, we ran test calculations for different initial conditions (different mean longitudes of Jupiter and the asteroids), but did not obtain the significant differences in the results which were discovered analytically by Henrard & Caranicolas (1990). Despite that disagreement, the analytical and numerical work may have solved the problem of the original depletion of asteroids in the 3:1 resonance. The qualitatively different behavior of the critical argument (circulation to libration) can cause large changes in the asteroid's orbit, which can then bring it close to Mars which ejects it from the resonance (see for details the quoted papers by e.g., Henrard, Dvorak, Wisdom and others). The inclination may play a much more important role here than in the resonance of the inner asteroid belt. We can see a very high RMS in the $\sigma(i)$-diagram for orbits with initially low eccentricity. In the RAD, no asteroids are found here.

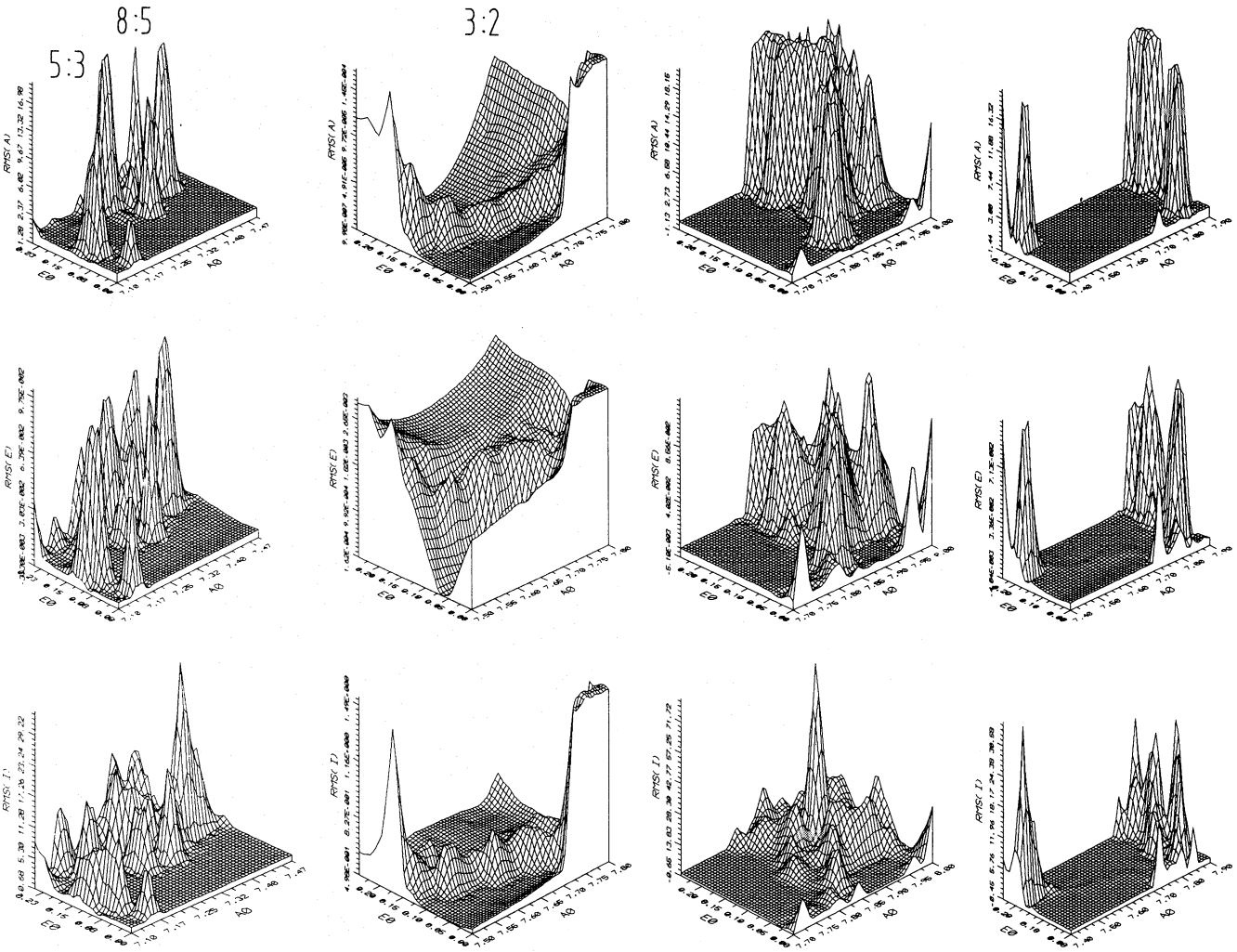

Fig. 9. Detailed picture of the dynamical structure of the main belt asteroids IV. The x-axis shows the initial semimajor axis in IU scale by a factor 10. The y-axis shows the initial eccentricity and the z-axis shows the mean standard deviation of the elements a, e, i. $\sigma(a)$ is cut off at 20 IU. In Fig. b $\sigma(a)$, $\sigma(e)$ and $\sigma(i)$ are cut off at lower values. Note: The scale of the z-axis differs from plot to plot

6.7. The 8:3 resonance (a = 0.520)

(Figure 7c): This resonance is present in the $\sigma(a)$-diagram with increasingly higher peaks along the y-axis (increasing initial e); the maximum value is $\sigma(a) = 2 \cdot 10^{-7}$. Again we see the inversion in $\sigma(e)$ starting with the initial e_o=0.1, which may lead to stabilization of an asteroid in this orbit. No significant feature can be seen up to $e_o \sim 0.12$ in the $\sigma(i)$-diagram. This resonance is visible in the RAD as a local minimum in the middle of the main belt (some hundred asteroids have semimajor axes close to it).

6.8. The 5:2 resonance (a = 0.543)

(Figure 7d): This resonance is noticeable as a broad mountain structure in all diagrams starting with $e_0 = 0.08$. The absolute values are also high ($\sigma(a)_{max} = 5 \cdot 10^{-6}$). The two characteristic peaks around $e = 0.17$ and $e = 0.23$ are present in all three diagrams. The inclination seems to be a very important parameter ($\sigma(i)_{max} = 18^o$). The triangle - like structure of the gap was already found by numerical integration (Yoshikawa 1991). This gap is very well established in the RAD, with sharp boundaries on both sides.

6.9. The 7:3 resonance (a = 0.568)

(Figure 8a): From the $\sigma(a)$-diagram one would conclude that our results confirm the real distribution: there rises a relatively broad mountain with increasing absolute heights starting with initial $e_o = 0.05$ on with $\sigma(a)_{max} = 2 \cdot 10^{-6}$. Examining the $\sigma(e)$-diagram, one notices the inversion of e which should be a small but nevertheless stabilizing factor. Note that the plot shows three (or maybe four) inversions in sequence. No significant perturbation is visible in the $\sigma(i)$-diagram. Summarizing the three graphs, suggests that no dynamical reason for the existence of the gap can be given when one compares the figures with the diagrams of other resonances (e.g. 5:2) The absolute σ values are quite small: more than 10 times smaller in $\sigma(i)$, 100 times

smaller in $\sigma(e)$ and 2 times smaller in $\sigma(a)$. Our results confirm those by Yoshikawa (1991), who also failed to explain the 7:3 resonance by the elliptic restricted model. Maybe the collision hypothesis (cf. Jefferys 1967; Giffen 1973; Lecar & Franklin 1973; Scholl & Froeschlé 1974) can give the correct answer. The gap in the RAD is also quite well defined (very similar to the 5:2 gap) and only few asteroids with a semimajor axis corresponding to that mean motion resonance are found.

6.10. The 9:4 resonance (a = 0.582)

(Figure 8b): There is no gap visible in the real distribution of the asteroids, although a secondary minimum between two peaks does exist. Looking at the $\sigma(a)$-diagram, we see a small increasing peak starting with e=0.1, which appears as inversion in the $\sigma(e)$-diagram. Nothing special is visible in the $\sigma(i)$-diagram. The slope on the right edge (towards Jupiter) on the $\sigma(a)$-diagram are is due to the nearness of the very broad 2:1 resonance.

6.11. The 2:1 resonance (a = 0.630)

(Figure 8b): The breadth of this gap is quite pronounced in the distribution of the real asteroids. Similarly to the 3:1 resonance, this was studied extensively by many authors with the aid of analytical models and numerical integrations (e.g., Sessin & Ferraz-Mello 1984; Henrard 1987; Murray 1986; Yoshikawa 1989, 1991). The structure of the gap is very interesting and unique: a very high chain of peaks of mountains, rises on the right edge, while on the left edge (towards Mars) one can recognize another chain of (lower) mountains. The whole structure forms a semicircle, with a smooth valley in the $\sigma(a)$-diagram, a small hill at the center of the $\sigma(e)$-diagram, and a plane in the $\sigma(e)$-diagram. As shown in Fig. 2, this bifurcation is the broadest for $M = 0^o$, while for $M = 90^o$ the two-branch structure degenerates into one line. Since the maximum value of σ in semimajor axis a is only $2 \cdot 10^{-4}$, the perturbations act such that they shift the asteroids from the central part of the resonance to the inner edge. It is visible also from the "Calculated Particle Distribution (Fig. 11) where one can see that the outer part of the resonance is empty, but the inner one is overpopulated in comparison to the original distribution. We have a very similar picture for the 2:1 resonance in the RAD. Mountains of stronger perturbations are also present there in the e- and i-diagrams. Because of the large valley in the middle and the smallness of the perturbations, it is not clear how the gap could form. Nevertheless, most of the recognizable features in the diagrams can be explained through a simplified analytical model (Henrard & Lemaitre 1987): the emergence of small chaotic layers on one hand and the crossing of a separatrix on the other. The question why there is lack of asteroids in the 2:1 resonance is still open (see 3:2 resonance).

6.12. The 9:5 resonance (a = 0.676)

(Figure 8c): This resonance is well pronounced in all three diagrams for $e_o \geq 0.2$, where a triple peak in $\sigma(a)$ rises. The corresponding perturbations act only as one high peak in $\sigma(e)$ and $\sigma(i)$. The RAD shows a well defined gap in this place.

Starting with this point, the picture becomes more and more complex and thus difficult to describe properly. We have already mentioned that several resonances may act very close to each other in the outer main belt.

6.13. The 7:4 resonance (a = 0.689)

(Figure 8d): Very strong perturbations occur in this resonance, even at small initial eccentricities. The complex structure is broad for greater values of e_o and even for small e_o we see several peaks which are already high. In the RAD, no asteroids are found in this resonance.

6.14. The 5:3 resonance (a = 0.711)

(Figure 9a): Acting only for small eccentricities this resonance lies in a plane of no perturbations. Close to the 5:3 resonance, different high-order resonances (in the form of the mountains) make the picture very difficult to interpret. This resonance is visible only for mean initial eccentricities $0.05 \leq e_o \leq 0.2$ and about the same structures are present in the $(\sigma(a) - \sigma(e) - \sigma(i))$ diagrams. The 5:3 gap is quite pronounced in the RAD, but according to our results it seems that different closely-spaced resonances may act to deplete the belt in the region between 0.7 and 0.724 .

6.15. The 8:5 resonance (a = 0.731)

(Figure 9a): Our plots show high perturbations in the form of mountains starting with e_o = 0.1 with a more or less different structure in all three plots. While four well distinguished peaks can be seen in $\sigma(a)$, the $\sigma(i)$-diagram shows a structured highland on the lower edge of the mountain and only one high peak on the outer edge. It is also present in the RAD (no asteroids have orbits at this semimajor axis).

6.16. The 3:2 resonance (a = 0.763)

(Figure 9a-d): One of the most exciting and still unsolved questions is the existence of the Hildas, a group of some 50 asteroids at this mean motion resonance with Jupiter. Much work has been devoted to this topic during recent years (e.g., Schubart 1979, 1982; Ferraz-Mello 1988) and interesting results were derived. They are easily visible in our plots, forming a well defined valley in all three representations ($a - e - i$). The mountains of the 8:5 resonance lie on the inner edge (for large initial values of the eccentricities). Far away (toward Mars), the perturbations caused by the 5:3 resonance (low eccentricities) enclose the Hilda-valley. On the outer edge, the broad zone of high order resonances causes different important perturbations, that are impossible to untangle in detail (because of the scales). We also calculated orbits of fictitious asteroids up to very close distances to Jupiter, but the picture becomes very inconclusive due to the phenomenon of the resonance overlap close to Jupiter (4:3, 5:4 etc.).

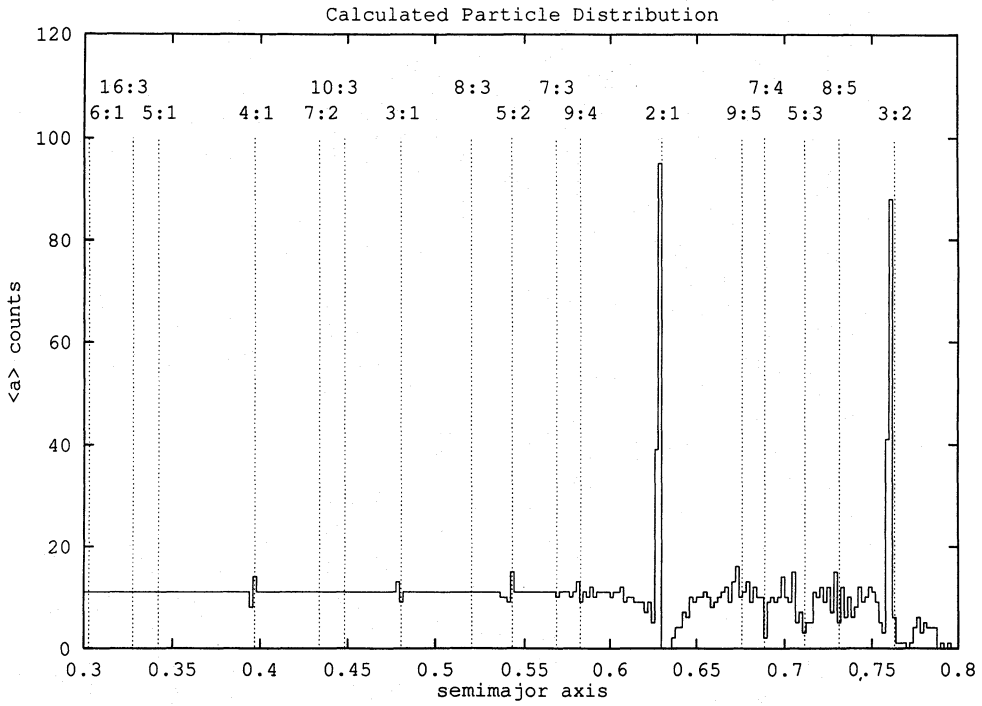

Fig. 10. Probability measure of the artifical asteroids. The resonances are indicated with dashed lines. Note the collection of particles at the 2:1 and 3:2 resonances

A closer view (Fig. 9b) shows that there are hills of perturbations in the Hilda valley which are, in fact, comparable in size to the hills in the 2:1 resonance. The right edge of the valley (Fig. 9c) has the form of a circular arc with some greater perturbations acting also for small e_o. This feature was also found by Wisdom (1987, Fig. 16) in the results of his numerical integrations and by Murray (1986, Fig. 9), derived with specially developed mapping techniques valid only for small eccentricities. Looking at the Fig. 11, we see that we have the same phenomenon as for the 2:1 resonance: the asteroids are shifted away from the center of the resonance to the inner edge, less to the outer edge. This characteristic is completely different from what we observe in reality: in the RAD we find the Hilda family exactly at the resonance and the edges are empty. Thus we are still far from having solved this intriguing problem of the 2:1 gap and the 3:2 family. We hope, however, that the inclusion of Saturn in the model for our numerical experiments will allow us to advance to a better understanding of this question.

7. Mean probability measure and final averaged distribution of the particles

For our numerical investigation of the dynamical structure of the main belt asteroids it is interesting to know the mean probability measure of the semimajor axes of the initially equally distributed fictitious asteroids. We therefore determined the mean semimajor axes for all the particles averaged over the whole integration time of $\sim 10^5$ years. We divided the semimajor axes between 0.3 and 0.8 in cells of breadth $\Delta a = 0.002$ and counted the number of asteroids with a mean semimajor axis falling into each of the cells. Without perturbations (Keplerian orbit) each cell would contain 11 particles. Figure 10 shows the result of this procedure: The characteristic feature is that either a gap or a peak is always present for each main mean motion resonance. It is also interesting to note that there are no particles at all between $a = 0.630$ and $a = 0.636$ and that there are deep gaps at the 7:4 and 5:3 resonances. The fictitious bodies have been gathered on one edge of each gap in the mean distribution representation. That mechanism acts relatively weakly in the 4:1, 3:1, 5:2, 9:4 gaps; it is most pronounced in the 2:1 and the 3:2 resonances through remarkably sharp peaks. In the two adjacent cells of $\Delta a = 0.004$ at the inner edge of these two gaps mentioned the concentration of particles has multiplied by 10 in comparison with what it was at the beginning. It is clear that collisions between the asteroids are expected there at this value of a, especially if the number of asteroids is sufficiently high. We believe that this mechanism is possibly working to deplete the 2:1 resonance (but our simulation is inconclusive because we did not allow collisions). The same argument does not hold for the 3:2 resonance because no asteroids should occur in that resonance also. Is is well known, however, (e.g., Ferraz-Mello 1988, 1990) that asteroids in high eccentric orbits in the 2:1 and 3:2 resonance are librating about one mean value $\langle a \rangle$ of the semimajor axis. This means that all asteroids with orbits with $e \geq 0.1$ will show this libration on a smaller scale and will produce the high peaks shown in the last figure with depletions on their borders. The depletion is much higher on the right edge due to the higher values of $\langle a \rangle$.

We also show the final distribution of the fictitious asteroids after 10^5 years (Fig. 11). Evidently, the picture is not a good representation of the RAD. Only a few resonances (3:1 and 5:3) appear as gaps. This is very probably due to different facts: 1. the model is incomplete; interactions other than those with Jupiter are not considered (the other planets, e.g. Saturn, may

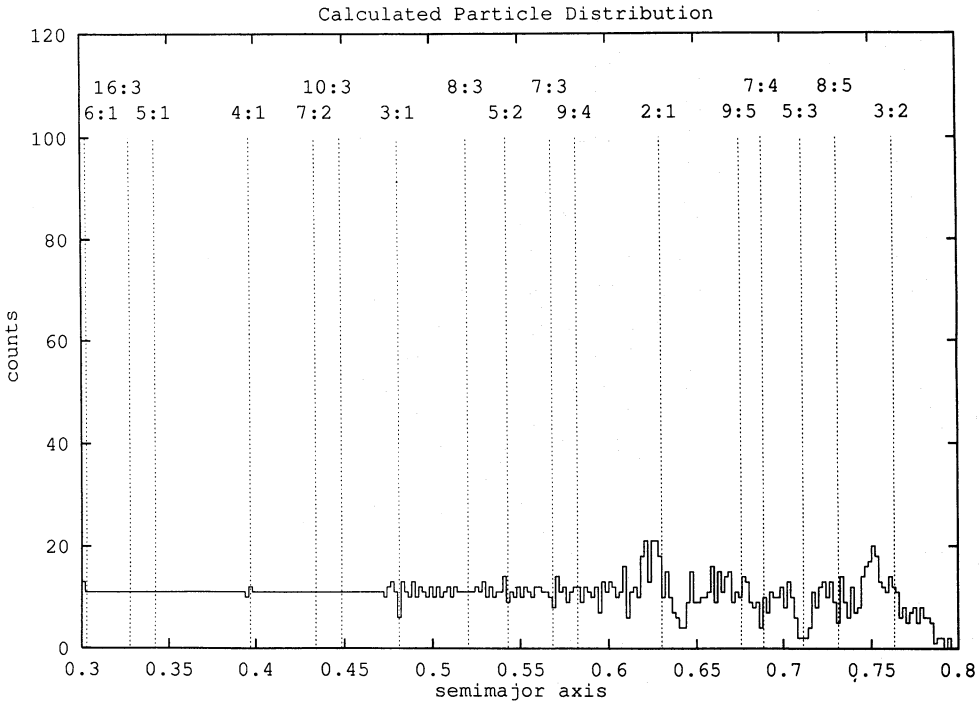

Fig. 11. Final distribution of the semi-major axis of the fictitious main belt asteroids. The resonances are indicated with dashed lines

be much more important than the interactions of the asteroids among themselves). Mars may thus play an important rôle also for the other gaps (as it does for the 3:1 gap).

2. the integration time scale is too small to represent the RAD (Fig. 1) and 3. The structure of the inner part of the belt in Fig. 11 does not resemble that of Fig. 1; the region between 0.3 and 0.4 should hold only about 3-4 percent of the entire population; consequently, it should be more or less depleted. The middle part of the belt from the 4:1 resonance to the 2:1 resonance does not replicate the structure of the RAD and does not contain more than 90 percent of the population of the main belt, as it does the real asteroid belt; even the gaps at the resonance are not conspicious. Neither do we find a good representation of the outer part of the belt between the 2:1 and the 3:2 resonances. It should contain about 6-7 percent of the whole asteroid population, but that part of the belt is also not depleted! There appears only a certain tendency to shift the asteroids toward the inner parts (to Mars).

Globally, Fig. 10 shows a more realistic picture than Fig. 11.

8. Discussion and conclusions

The main purpose of this paper is to investigate, for the first time, the dynamical structure of the entire main belt of asteroids. Due to our limited computer resources we restricted the dynamical model and the integration time and also the grid of the initial conditions. Nevertheless, comparing our results with new ones for the outer belt we found a satisfying agreement.

In a long term integration (up to 22.5 million years) with a newly developed symplectic integrator algorithm Gladman & Duncan 1990 (=GD) concentrated on asteroid motion in the outer solar system: the outer main belt asteroids, the region between Jupiter and Saturn and possible asteroids outside Saturn's orbit. For the outer asteroid belt ($0.6 \leq a \leq 0.75$) GD determined the removal time of 80 test particles with initially circular orbits under the gravitational influence of Jupiter and Saturn. GD found that one half of the asteroids was removed due to a close approach to Jupiter and the other half due to encounters with Mars. The removal time for such fictitious asteroids from the outer belt is given in GD's Fig. 6a; in their Fig. 6b the initial semi-major axis of the asteroids is plotted versus the semi-major axis at the end of 12 million years of integration. Both graphs nicely show the locations of the main resonances in the outer belt region mentioned above. The visible structure of the 2:1 resonance in Fig. 6a reflects a feature which is also present in our Fig. 8a,b and c: in their plots one can see that on the inner side of the resonance the removal time is significantly longer (one high peak) than on the outer side (the three shorter bars on the outer side correspond to shorter removal times). In our graphs the strength of the perturbations in a resonance is visible through peaks of the mean standard deviation. The inner edge of the 2:1 resonance (Fig. 8) shows smaller peaks, while higher peaks are clearly visible on the outer edge of the 2:1 resonance. The resonances 9:5, 7:4, 5:3 and 8:5 are easily identified in Fig. 6a and 6b of GD as well as in our Fig. 3 ($\sigma(a)$), Fig. 4 ($\sigma(a)$), and Fig. 5 ($\sigma(a)$) where a the semi-major axis, e the eccentricity and i the inclination of the orbit of the fictitious asteroid. According to our graphs the 7:4 resonance seems to be the strongest one. This is not in agreement with the results of GD where the 5:3 resonance appears as the strongest one (besides the 2:1). One more remark should be made: In our Figs. 3, 4, and 5 we also recognize that the perturbations in the outer part of the belt are not acting at the exact resonance but somewhat outside; this fact

coincidences with the result of GD that "the clearing occurs just outside the exact commensurability".

New results of extensive numerical integrations were published by Lecar et al. (1992) (=LEL) for the orbits of 140 fictitious asteroids with semi-major axes between 0.63 and 0.76 ($a_{Jupiter}$ = 1). These calculations were carried out in the plane problem taking into account the variations of the eccentric orbit of Jupiter and the rotation of its line of apsides for time intervals of 1 million Jovian years. LEL were primarily interested in the explanation of the absence of asteroids in this region (only 1 promille out of all main belt asteroids have orbits with semimajor axis in this regarded region). They found that approximately 70 per cents of their sample (with $0.68 \leq a \leq 0.74$) were ejected after a close approach to Jupiter. As mentioned in the comparison with GD in our Figs. 3, 4, and 5 one can recognize the strong perturbations acting on asteroids in this region due to resonances with Jupiter (9:5, 7:4, 5:3 and 8:5). In order to see whether asteroids possibly could be ejected we must look at the largest eccentricity values achieved during the integration time. Unfortunately a check with our own results is only possible for asteroids in the 2:1 resonance where respective diagrams are published (Dvorak 1992a, 1992b). There we can see that, according to the eccentricities achieved, only a small percentage in the 2:1 resonance could be ejected due to a close approach with a planet (primarily Jupiter).

Our data presented here cover the whole main belt of asteroids and not only the outer part; comparing our results with reality we can say that they reflect the main dynamical properties of the main belt asteroids. Figs. 3, 4 and 5 show the distribution of $\sigma(a)$, $\sigma(e)$ and $\sigma(i)$ combined for all initial eccentricities. Only the main resonances are visible due to the different scales. The best representation is the $\sigma(a)$ plot, where we also recognize the high-order resonances in the logarithmic plot. Almost all the gaps in the inner belt are represented through peaks in $\sigma(a)$; moving outward from the 2:1 resonance we detect local minima for the $\sigma(a)$ at exactly the location of the resonances.

Taking into account the different initial eccentricities (Figs. 6 to 9) we see, that the resonances form more or less triangles with the top on the side of the small e_o. In these resonances the asteroids are thus perturbed out to the edges of the resonance.

Finally, we emphasize some important results of these numerical experiments concerning the dynamical structure of the asteroids between Mars and Jupiter:

- All the main gaps are well visible in all diagrams
- There is a certain tendency to push the asteroids from the outer to the inner part of the belt away from Jupiter.
- The structure of the 2:1 resonance is confirmed as most of the asteroids from the outer edge of this resonance are pushed toward the inner part. This characteristic asymmetry is also found in the RAD.
- The asymmetric structure of the distribution is also visible in the 3:2 resonance (an accumulation of asteroids on the inner part of the resonance is also visible the RAD).

Returning once more to Fig. 11 which shows the final distribution of the fictitious asteroids after 10^5 years. Our results would probably have replicated the RAD if we would have lenghtened the time scale of integration by a factor of 5 to 10 (up to 10^6 Jupiter revolutions). Even more important would be a more realistic model including Saturn and possibly Mars in our calculations. The main purpose of the present study was, however, to investigate only the gravitational influence of Jupiter on the structure of the belt, taking into account also the inclinations of the orbits. When we proceed to the next, more realistic model (with Saturn) we hope to isolate Saturn's rôle on the structure of the belt and, step by step, also the rôle of the other planets.

And last but not least, it was our purpose to contribute to a better understanding of the complexity of the dynamics of the main belt asteroids with its intriguing structure of gaps and families.

Acknowledgements. First of all we have to express our thanks to Prof. Contopoulos for his great help to improve the presentation of our results. We are also grateful to Prof. Eichhorn for correcting the English text. For discussions during their stay at the Vienna observatory concerning the problem of the dynamics of asteroids in connection with our results we thank Prof.Sun from Nanking University and Prof.Ferraz-Mello from Sao Paulo. We also thank Prof. P. Stumpff and Dr. M. Bird (RAIUB) for valuable advice in writing the paper. Finally we must thank the MPI für Radioastronomie for the use of their fast computer facilities.

References

Bock, H.G., 1987, Bonner Mathematische Schriften 183,
Bock,H.G., Eich,E., Schloder,J.P., 1988, In: Strehmel (ed.) Numerical Treatment of Differential Equations, BG Teubner, Leipzig, 45
Bulirsch R., Stoer J., 1966, Numerical Treatment of Ordinary Differential Equations by Extrapolation Methods, Numerische Mathematik 8, 1-16
Chirikov, B.V., Vecheslavov, V.V., 1986, Preprint 86-184, Institute of Nuclear Physics, Novosibirsk
Dvorak R., 1992a, In: Ferraz-Mello S. (ed.), IAU Symposium 152 Chaos, Resonance and Collective Dynamical Phenomena in the Solar System, 145
Dvorak, R., 1992b, Celest. Mech, 54, 195
Dvorak, R., Kribbel J., 1990, A&A 227, 264
Dvorak, R., Lohinger E., 1991, In: Roy, A.E. (ed.) Predictability, Stability, and Chaos in N-Body Dynamical Systems, NATO ASI Series, Plenum Press, New York, 439
Ferraz-Mello, S., 1987, In: Šidlichovský M. (ed.) Dynamics of the Solar System, Astron.Inst.Czech.Acad.Sciences, Praha, 121
Ferraz-Mello, S., 1988, AJ 96, 400
Ferraz-Mello, S., 1990, Revista Mexicana Astron.Astrofisica 21, 569
Ferraz-Mello, S., Klafke, J.C., 1991, In: Roy, A.E. (ed.) Predictability, Stability, and Chaos in N-Body Dynamical Systems, NATO ASI Series, Plenum Press, New York, 177
Froeschlé, Cl., 1984, Celest. Mech. 34, 95
Froeschlé, Cl., Gonczi R., 1988, Celest. Mech. 43, 325
Froeschlé, Cl., Scholl H., 1981, A&A 93, 62
Froeschlé, Cl., Scholl H., 1982, A&A 111, 346
Giffen, R., 1973, A&A 23, 387
Gladman, B., Duncan, M., 1990, AJ 100, 5, 1680
Hadjidemetriou, J.D., 1986, J.Appl.Math.Phys. 37, 776
Hadjidemetriou, J.D., 1991, In: Roy, A. (ed.), Predictability, Stability, and Chaos in N-Body Dynamical Systems, 157

Hadjidemetriou, J.D., 1988, In: Roy, A. (ed.), Long Term Behaviour of Natural and Artificial N-Body Systems, Kluwer Academic Publishers, 257
Hadjidemetriou, J.D., Ichtiaroglou, S. , 1984, A&A 131, 20
Hanslmeier, A., Dvorak R., 1984, A&A 132, 203
Henrard, J., 1988, In: Roy, A. (ed.), Long Term Behaviour of Natural and Artificial N-Body Systems, Kluwer Academic Publishers, 405
Henrard, J., Caranicolas N.D., 1990, Celest. Mech. 47, 99
Henrard, J., Lemaitre A., 1986, Celest. Mech. 39, 213-238
Henrard, J., Lemaitre A., 1987, Icarus 69, 266
Jefferys, W.H., 1967, AJ 72, 872
Kallrath, J., 1992, Celest. Mech., (in press)
Klafke, J.C., Ferraz-Mello, S,, Michtchenko, T.: 1992, In: Ferraz-Mello S. (ed.), IAU Symposium 152 Chaos, Resonance and Collective Dynamical Phenomena in the Solar System, 153
Laskar, J., 1987, In: Šidlichovský M. (ed.) "Dynamics of the Solar System", Astron.Inst.Czech.Acad.Sciences, Praha, 121
Lecar, M., Franklin F.A., 1973, Icarus 20, 422
Lecar, M., Franklin F.A., Soper, P., 1992, Icarus 96, 234
Lemaitre, A., Henrard J., 1990, Icarus 83, 391-409
Morbidelli, A., Giorgilli, A., 1990, Celest. Mech. 47, 173
Murray, C.D., 1986, Icarus 65, 70
Murray, C.D., Fox K., 1984, Icarus 59, 221
Petrosky, T.Y. , Broucke, R.: 1988, Cel.Mech. 42, 53
Scholl, H., 1979, In: Duncombe,R.L. (ed.), IAU Symposium 81, Dynamics of the Solar System, Reidel, Dordrecht, 217,
Scholl, H., 1985, In: Ferraz-Mello S., Sessin, W. (eds.) Resonances in the Motion of Planets, Asteroids and Satellites. Univ. of Sao Paulo, 129
Scholl, H., Froeschlé, Cl., 1975, A&A 42, 457
Schubart, J., 1968, AJ 73, 99
Schubart, J., 1979, In: R.L. Duncombe (ed.) Dynamics of the Solar System, IAU Symposium No. 81, 207
Schubart, J., 1982, A&A 114, 200
Schubart, J., Stumpff P., 1966, Veröffentl. Astron. Recheninst. Heidelberg Nr.18
Sessin, W., Ferraz-Mello, S., 1984; Celest. Mech. 32, 307
Sidlichovský, M., 1992a, A&A 259, 341
Sidlichovský, M., 1992b, Chaotic behaviour of trajectories for the fourth and third order asteroidal resonances, (in press)
Szebehely, V., 1970, Theory of Orbits. Academic Press Inc., Orlando, 587ff
Wisdom, J., 1982, AJ 87, 577
Wisdom, J., 1983, Icarus 56, 51
Wisdom, J., 1987, Icarus 72, 241
Yoshikawa, M., 1989, A&A 213, 436
Yoshikawa, M., 1990, Icarus 87, 78
Yoshikawa, M., 1991, Icarus 92, 94

This article was processed by the author using Springer-Verlag LaTeX A&A style file version 3.